Boron-doped microporous nano carbon as cathode material for high-performance Li-S batteries

Feng Wu[1,2,§], Ji Qian[1,§], Weiping Wu[3], Yusheng Ye[1], Zhiguo Sun[1], Bin Xu[4], Xiaoguang Yang[5], Yuhong Xu[6], Jiatao Zhang[7], and Renjie Chen[1,2] (✉)

[1] *Beijing Key Laboratory of Environmental Science and Engineering, School of Material Science and Engineering, Beijing Institute of Technology, Beijing 100081, China*

[2] *Collaborative Innovation Center of Electric Vehicles in Beijing, Beijing 100081, China*

[3] *School of Computer Science, Mathematics and Engineering, City, University of London, Northampton Square, London, EC1V 0HB, UK*

[4] *State Key Laboratory of Chemical Resource Engineering, Beijing Key Laboratory of Electrochemical Process and Technology for Materials, Beijing University of Chemical Technology, Beijing 100029, China*

[5] *Research and Advanced Engineering, Ford Motor Company, MI 48121, USA*

[6] *Electrified Powertrain Engineering, Ford Motor Research and Engineering (Nanjing) Co. Ltd., Nanjing 211100, China*

[7] *Beijing Key Laboratory of Construction-Tailorable Advanced Functional Materials and Green Applications, School of Material Science and Engineering, Beijing Institute of Technology, Beijing 100081, China*

[§] *These authors contributed equally to this work.*

ABSTRACT

In this study, a boron-doped microporous carbon (BMC)/sulfur nanocomposite is synthesized and applied as a novel cathode material for advanced Li-S batteries. The cell with this cathode exhibits an ultrahigh cycling stability and rate capability. After activation, a capacity of 749.5 mAh/g was obtained on the 54th cycle at a discharge current of 3.2 A/g. After 500 cycles, capacity of 561.8 mAh/g remained (74.96% retention), with only a very small average capacity decay of 0.056%. The excellent reversibility and stability of the novel sulfur cathode can be attributed to the ability of the boron-doped microporous carbon host to both physically confine polysulfides and to chemically bind these species on the host surface. Theoretical calculations confirm that boron-doped carbon is capable of significantly stronger interactions with the polysulfide species than undoped carbon, most likely as a result of the lower electronegativity of boron. We believe that this doping strategy can be extended to other metal-air batteries and fuel cells, and that it has promising potential for many different applications.

1 Introduction

Rechargeable batteries are extensively used in numerous portable devices and electric vehicles; however, the energy density of Li-ion batteries cannot satisfy the increasing demand for energy storage. Therefore, a

new generation of batteries with a high energy density and a long cycle life is in urgent demand [1]. Among the various promising candidates, the lithium-sulfur (Li-S) battery is the most promising electrochemical system because of its high theoretical specific capacity (1,672 mAh/g) and high energy density (2,600 Wh/kg) [2]. In addition, the sulfur active material is low cost, highly abundant, and nontoxic, which makes Li-S batteries even more attractive. Despite these advantages, the commercialization of Li-S batteries has not been realized because of several technical bottlenecks, such as the insulating nature of sulfur and lithium sulfide and the dissolution of polysulfides, which results in poor reversibility and stability of Li-S batteries [3, 4].

To solve these challenges, conceptually new materials and rational design of the electrode structure are essential [5, 6]. Over the past years, cathode materials that incorporate sulfur into different carbon matrices, especially into carbon nanomaterials (including carbon nanotubes [7–9], graphene [10–13], and porous carbon [14–16]) and carbon-based hybrids were developed in order to improve the electrical conductivity and to accommodate the electrode volume expansion during the cell operation. Specifically, sulfur-coated carbon nanotubes (CNTs) [17] have been widely applied in Li-S batteries. In these batteries, the surface of CNTs is coated with sulfur to produce a core–shell structure. The major challenges associated with these undoped carbon-based Li-S batteries are the fast capacity decay, low coulombic efficiency, and poor rate capability. Further modifications of the cathode are still underway. For example, Chen et al. treated CNTs with nitric acid in order to incorporate carboxyl functional groups, and the resulting CNTs/sulfur cathode delivered a comparatively improved electrochemical performance [18]. Nevertheless, the relatively low surface area and pore volume of CNTs present an inherent problem for the CNT/S cathode.

Elemental doping of carbon nanomaterials has attracted significant attention, mainly due to the excellent electrochemical catalytic activity of these materials for many applications. Boron and nitrogen are two of a small group of elements, which can be used to substitutionally dope graphene structures, thereby improving the electronic and structural properties. Furthermore, boron-doped carbon as a key promising electrode material presents a new platform for energy storage applications, especially for Li-S batteries.

Herein, we designed and synthesized novel boron-doped carbon nanostructured material from CNTs. The nanotubes in the obtained material have a unique coaxial structure, with boron doped in the surface layer of carbon. The obtained boron-doped microporous carbon (BMC) possesses a large surface area. Moreover, due to the low electronegativity of boron, the electronic properties of the B-doped sites are expected to be altered [19, 20]. Additionally, the created active sites tend to attract polysulfides, thus helping to alleviate the shuttle effect. Therefore, BMC can effectively impregnate sulfur and trap the soluble polysulfides generated during the charge–discharge processes.

2 Experimental

2.1 Preparation of composite materials

2.1.1 Preparation of BMC

Raw multi-walled carbon nanotubes (120 mg) (Aligned-MWCNT, 10-30 nm in diameter, Shenzhen Nanotech Port Co. Ltd, China) were refluxed in concentrated HNO_3 at 120 °C for 5 h and then washed with distilled water. The modified CNTs were dispersed in water (30 mL) containing sodium dodecyl sulfate (12 mg) to give a black CNT suspension. For the synthesis of BMC, glucose (4.8 g) and boric acid (6 g) were first dissolved in water (30 mL), followed by addition of the CNT suspension. The obtained homogeneous black suspension was sealed in a PTFE container and maintained in an oven at 190 °C for 15 h. The product was collected by vacuum filtration and dried in a vacuum oven at 60 °C for 24 h. The product was then completely carbonized at 800 °C for 3 h under a flow of argon, affording the target BMC as a black powder.

2.1.2 Preparation of BMC/S composite

Sulfur (Alfa Aesar) and BMC (in a 7:3 and 6:4 ratio by mass for two different recipes, respectively) were mixed and sealed in an iron pot, and heated to 155 °C in an oven for 24 h under Ar atmosphere. The resulting

composites are referred to as BMC/HS and BMC/LS, respectively.

2.1.3 Preparation of CNT/S composite

As a comparison, sulfur and aligned multiwalled CNTs (7:3 ratio by weight) were mixed and sealed in an iron pot, followed by heating to 155 °C in an oven for 24 h under Ar atmosphere.

2.2 Characterization and computational methods

In order to determine the boron content in the prepared BMC material, BMS was dissolved completely by digestion and analyzed using inductively coupled plasma-optical emission spectroscopy (ICP-OES, Varian Vista-MPX CCD Simultaneous). Nitrogen sorption isotherms were obtained at 77.2 K using an ASAP 2460 Surface Area and Porosity Analyzer (Micromeritics). Mass of the samples analyzed in this measurement was 35.9 and 49.2 mg for BMC and CNTs respectively. Calculation of the pore-size distribution was performed using non-localized density functional theory (NLDFT), using the adsorption branch for CNTs and the Horvath–Kawazoe (H–K) method for BMC. Thermogravimetric analysis (TGA) of the cathode material was carried out using a thermogravimetric/differential thermal analysis (TG/DTA) system (EXSTAR 6200, Japan) at a heating rate of 10 °C/min under Ar atmosphere. X-ray photoelectron spectroscopy (XPS, ESCALAB 250) was performed using a monochromatized Al Kα radiation. Raman spectra were measured using a spectrometer (Renishaw-1000, UK) with an excitation wavelength of 532 nm. X-ray diffraction (XRD) patterns were recorded on a Rigaku X-ray diffractometer (Ultima IV-185, Japan) with Cu Kα radiation (λ = 0.154 nm). Particle morphologies were observed by field-emission scanning electron microscopy (FESEM, FEI Quanta 250, USA) and high-resolution transmission electron microscopy (HRTEM, JEOL-2010, Japan). Elemental analyses were conducted using an attached energy dispersive X-ray (EDX) apparatus.

The binding energy (BE) of the polysulfides adsorbed on the carbon surface was obtained by taking the energy difference between the energies (E) of the isolated Li_2S_3 and the B-doped (or undoped) carbon and the energy of the absorbed system. Namely, the binding energy is obtained using BE = $E_{(graphene)}$ + $E_{(Li2S3)}E_{(total)}$. The charge distribution on each atom was evaluated using a Mulliken population analysis. Geometry optimizations were carried out with the all-electron, density functional theory (DFT) program DMol3 in Materials Studio 5.5 (Accelrys), using the Becke–Lee–Yang–Parr (BLYP) functional and the Gaussian double zeta numerical plus polarization (DNP) basis set. An optimization was considered converged when the following convergence criteria were met: 1.0×10^{-5} Ha for the total energy, 0.002 Ha/Å for the maximum force on atoms, and 0.005 Å for the maximum atomic displacement.

2.3 Electrochemical measurements

The prepared composites were each formed into a cathode slurry. The composite (70 wt.%), acetylene black (20 wt.%), and polyvinylidene fluoride (10 wt.%) in N-methyl-2-pyrrolidinone (NMP) were mixed, and then ball-milled for 4 h to give a homogeneous slurry. After stirring, the slurry was coated in aluminum foil using a roll press. The coated electrodes were dried in a vacuum oven at 60 °C for 24 h. The electrodes were cut into discs with a diameter of 11 mm. The sulfur loading is about 1 mg/cm^2. Two-electrode coin cells (CR2025) with lithium foil counter electrodes were assembled in an argon-filled glove box. The employed electrolyte constituted of 1.0 mol/L lithium bis(trifluoromethane)sulfonimide (LiTFSI, TCI) and 0.2 mol/L lithium nitrate ($LiNO_3$, Alfa Aesar) in dimethoxyethane (DME) and 1,3-dioxolane (DOL) solvents (1:1 v/v, Alfa Aesar). The volume of the electrolyte added into the cells was 50 μL. The cells were discharged and charged over the voltage range 1.7–2.8 V at different current densities. An electrochemical station (Wuhan LAND electronics, China) was used to test the cycling stability of each cell. To characterize the redox behavior and kinetic reversibility of the cells, cyclic voltammetry (CV) curves were recorded on a CHI660c electrochemical workstation (Shanghai Chenhua, China) from 1.0 to 3.0 V. Alternating current (AC) impedance was measured with a CHI660c electrochemical workstation. The AC amplitude was ±5 mV and the applied frequency range was 0.1–100 kHz.

3 Results and discussion

In the synthesis of BMC, the raw CNTs are used as the scaffolding, providing the surface (Scheme 1) necessary for the formation of the boron-doped carbon layer, generated through the carbonization of glucose and boric acid. The boron content in BMC was determined by ICP-OES as 0.78 wt.%. The low magnification SEM images of BMC shown in Fig. S1 in the Electronic Supplementary Material (ESM), indicate that the obtained BMC grows well and homogeneously. Figures 1(a) and 1(b) represent the SEM images of the raw CNTs and BMC, respectively.

From this figure, it can be noticed that BMC retains its tubular morphology even after being coated with the boron-doped carbon layer. As clearly shown in the inset of Fig. 1(b), the diameter of BMC is ca. 200 nm, while the diameter of the original CNTs is only 10–30 nm. This difference demonstrates that the main body of BMC is composed of the boron-doped carbon layer. As we expected, the specific surface area (based on the Brunauer–Emmett–Teller method) of BMC has increased significantly (Fig. 1(d), 461.73 m^2/g) relative to that of CNTs (Fig. 1(c), 163.85 m^2/g). The adsorption isotherm for BMC is a type I isotherm, with a nitrogen adsorption plateau and no hysteresis, features indicative of micropore-rich structures [21]. Moreover, according to the pore size distribution plot obtained using the H–K method, the pores in BMC are predominantly micropores (Fig. 1(f)), with a pore size of about 0.34 nm. These micropores differ greatly from those present in raw CNTs (Fig. 1(e)). This unique porous structure of BMC can significantly improve the ability of the electrode to trap soluble polysulfides.

The sulfur-BMC composites were prepared using the thermal treatment method, which has been widely used in the fabrication of sulfur composites [22, 23]. The sulfur contents of BMC/HS and BMC/LS composite samples were confirmed (Fig. S2 in the ESM) by thermogravimetric analysis as 67 wt.% and 59 wt.%, respectively. In the following discussion, BMC/LS composite is mainly used for the structural characterization. Figures 2(a) and 2(b) show the SEM images of BMC/LS composite, with no visible sulfur bulk. In contrast, sulfur bulk is still visible in the composite that is heat-treated for only 8 h (Fig. S3 in the ESM).

These SEM images reveal that full incorporation of sulfur into the BMC-based matrix has been achieved in the BMC/LS composite. In the TEM image of BMC/LS composite shown in Fig. 2(c), a coaxial structure can be clearly identified, as marked with white dotted lines. On the other hand, the lattice strings of CNTs can be hardly observed in the HRTEM image (Fig. S4 in the ESM), due to their extremely

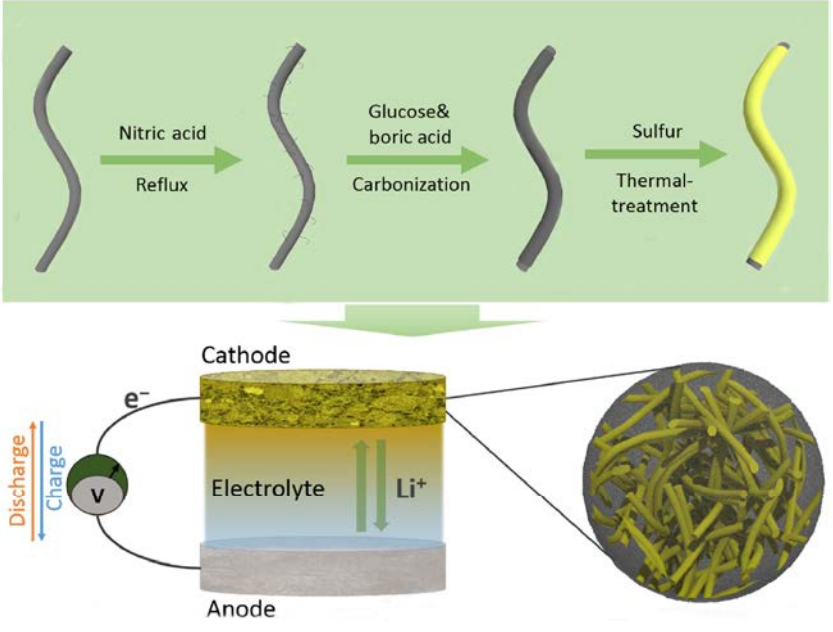

Scheme 1 Schematic illustration of the synthetic route to BMC.

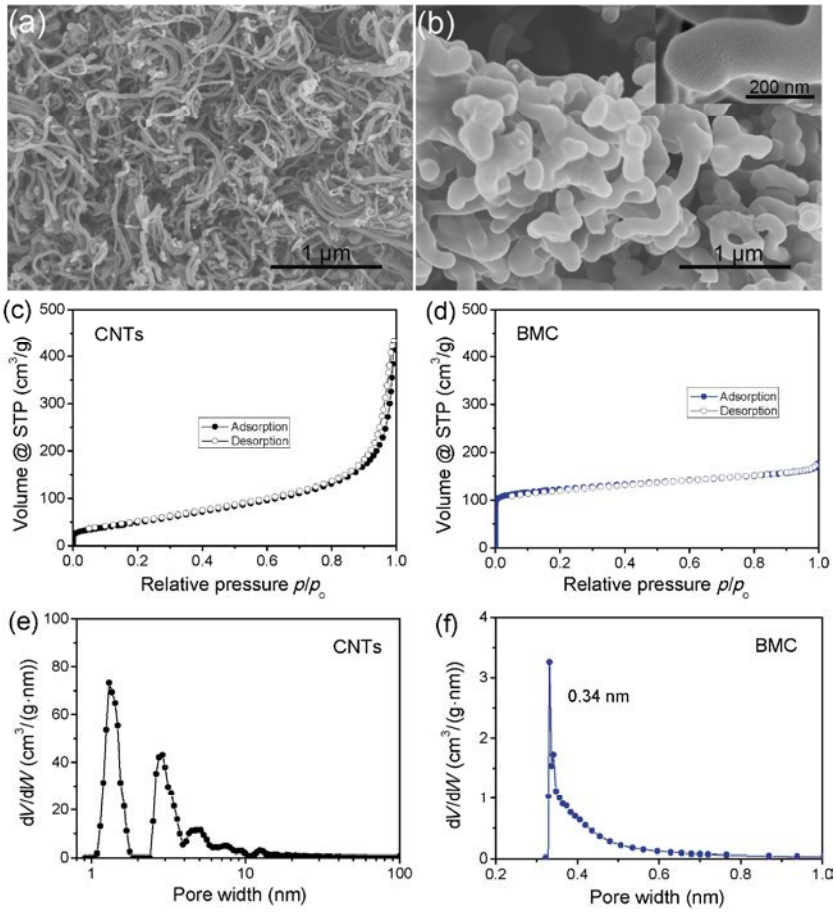

Figure 1 SEM images of (a) CNTs and (b) BMC, and the corresponding nitrogen sorption isotherms for (c) CNTs and (d) BMC; (e) the pore size distribution determined for CNTs using NLDFT method and (f) the pore size distribution determined for BMC using H–K method.

small diameter compared to that of BMC. According to the corresponding EDX elemental maps of the region marked with a black rectangle, sulfur is uniformly distributed in the boron-doped carbon layer.

The BMC/LS composite has been characterized using XRD, XPS and Raman spectroscopy. XRD patterns of sulfur, BMC, BMC/LS and BMC/HS composites are shown in Fig. 3(a). Overall, the sulfur-BMC composites exhibit a pattern similar to that of sulfur, which confirms that the sulfur in the composite is highly crystalline. Raman spectrum of the BMC/LS composite (Fig. 3(b)) shows three characteristic peaks: G band at ~1,593 cm^{-1}, D band at ~1,352 cm^{-1}, and 2D band at ~2,704 cm^{-1}. The G band is usually assigned to the E_{2g} phonon of sp^2 C atoms, while the D band is assigned to the defects and disorder in the carbon structure [24]. For the BMC/LS composite, the intensity ratio of the D band to the *G* band (I_D/I_G) is about 0.9656, which is slightly larger than the ratio for CNT/S (Fig. S5 in the ESM). This value indicates that the aromatic structures in BMC [25] remain largely intact, and their presence will aid the electron transport within the BMC/LS composite. In addition, the peak at ~472 cm^{-1} is the peak characteristic for sulfur, and is assigned to the A1 symmetry mode of the S–S bond [26].

As shown in the XPS spectra of the S 2p regions (Fig. 3(c)), two distinct peaks at 163.9 eV (S 2p3/2) and 165.1 eV (S2p1/2) appear, while the C 1s peak is located at 284.8 eV (Fig. 3(c), inset). Moreover, the binding energy of the B 1s peak is located at 190.9 eV (Fig. 3(d)), which is higher than the standard value (188.0 eV) [27], indicating that the boron atoms are bonded to the carbon atoms in the sp^2 carbon network [28]. Additionally, it is evident that the broad peak is composed of several smaller sub-peaks, corresponding to the heterocyclic structures illustrated in the inset

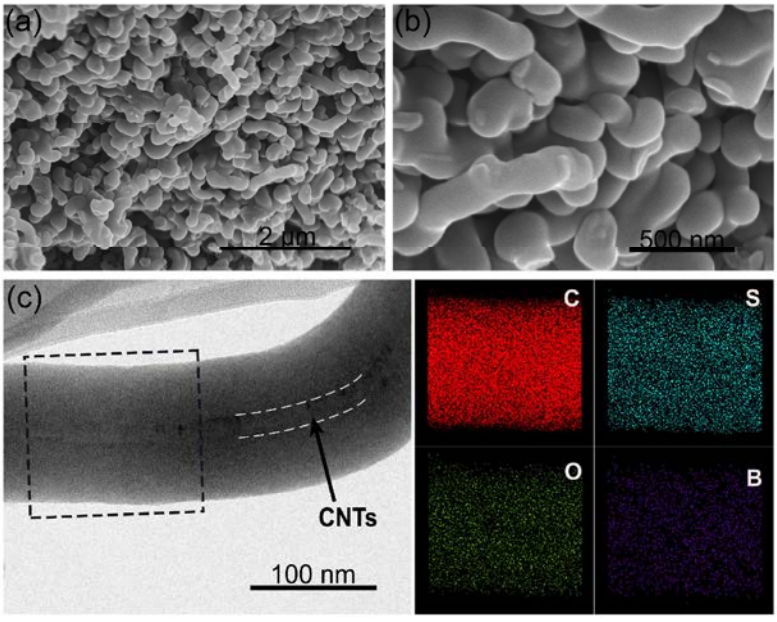

Figure 2 (a) and (b) SEM images of BMC/LS composite. (c) TEM image of the BMC/LS composite and the corresponding EDX elemental maps of the region marked with a black rectangle.

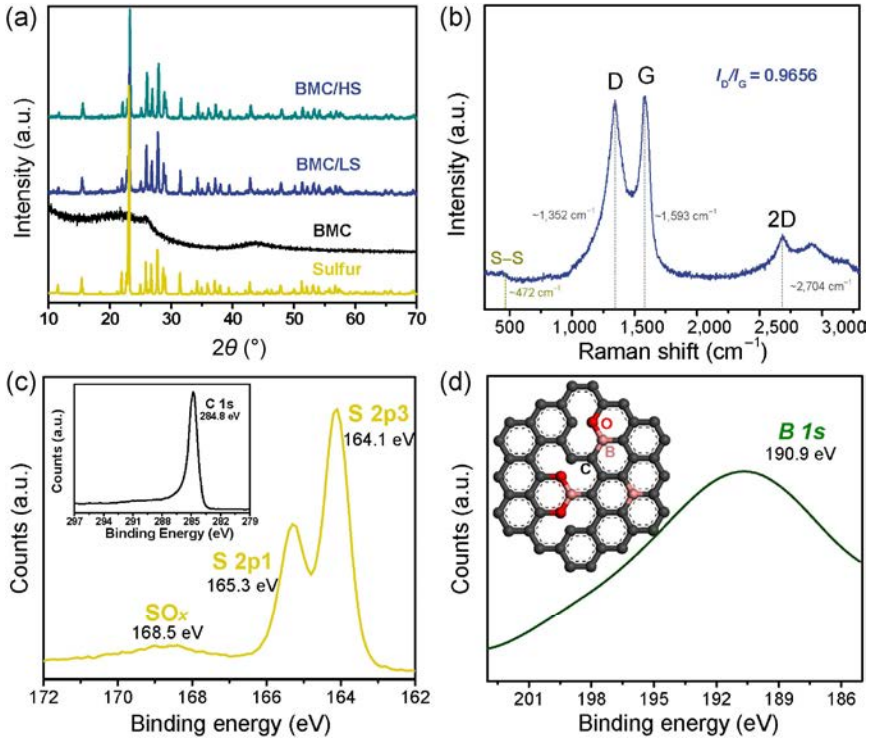

Figure 3 (a) XRD patterns of sulfur, BMC, BMC/LS and BMC/HS. (b) Raman spectrum of the BMC/LS composite and XPS spectra of (c) S 2p regions and (d) B 1s region of the BMC/LS composite. The inset in (c) represents the C 1s region.

of Fig. 3(d) [29].

In order to investigate the electrochemical properties of the composites, coin cells were assembled, with the composite and lithium foil as the cathode and anode, respectively. AC impedance measurements were performed on these cells prior to cycling, as shown in Fig. 4(a). We chose a typical model for the analysis of the Nyquist plots, and the results are

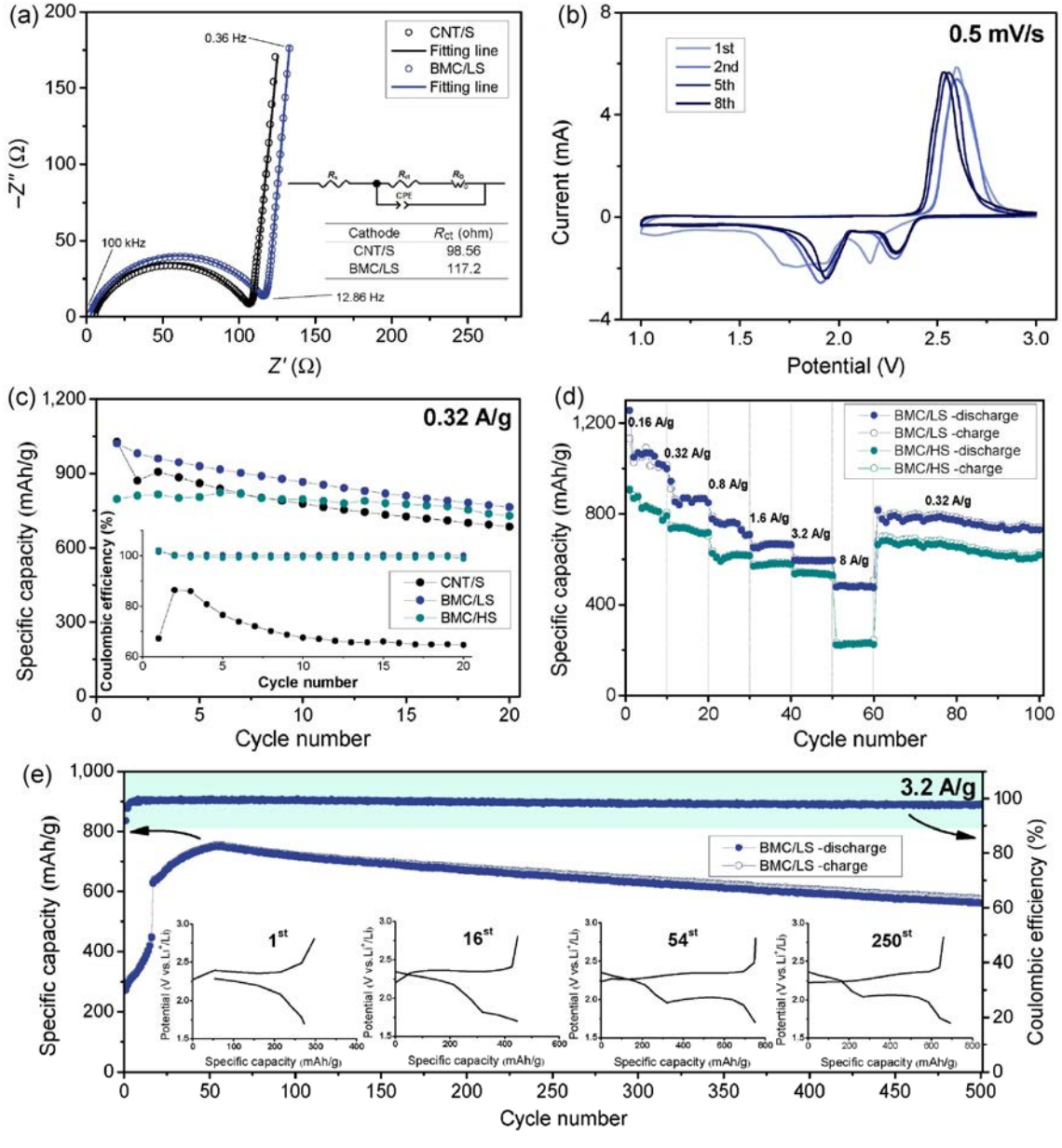

Figure 4 (a) AC impedance measurements of the cells with BMC/LS, and CNT/S cathodes prior to cycling. (b) Cyclic voltammetry curves of the BMC/LS cathode at a scanning rate of 0.5 mV/s. (c) Cycling stability of cells containing CNT/S, BMC/LS, and BMC/HS cathodes at 0.32 A/g. (d) Rate capabilities of BMC/LS and BMC/HS cathodes. (e) Cycle performance of BMC/LS cathode at 3.2 A/g (the insets show the discharge/charge voltage profiles on certain cycles). The sulfur contents of BMC/LS, BMC/HS, and CNT/S are 59 wt.%, 67 wt.%, and 60 wt.%, respectively.

displayed in Fig. 4(a). The analysis revealed that the R_{ct} value of BMC/LS is slightly higher than that of the CNT/S composite. This difference demonstrates the lower electrical conductivity of the BMC/LS composite, which may be caused by a minor structural damage to the boron-doped carbon layer during carbonization. Figure 4(b) shows the cyclic voltammetry curves of the BMC/LS cathode in the potential window of 1.0 to 3.0 V, at a scanning rate of 0.5 mV/s. Two separate cathodic peaks can be observed, which correspond to the reduction of elemental sulfur to lithium polysulfides and further reduction of polysulfides to Li_2S_2/Li_2S, respectively [30]. It is worth noting that, a conspicuous broad peak at 1.7 V appeared in the first cycle, which corresponds to the reduction of $LiNO_3$ [31].

The cycle performance of CNT/S, BMC/LS, and

BMC/HS cathodes at 0.32 A/g is shown in Fig. 4(c). Predictably, the CNT/S cathode delivers a lower capacity than the BMC/LS and BMC/HS cathodes after 6 cycles, indicating that a smaller quantity of active material is being used. The Coulombic efficiency of the cell containing the CNT/S cathode declines significantly to 65% after 20 cycles, while the BMC/LS and BMC/HS cathodes remain at ca. 99%. These results suggest that soluble polysulfides can migrate from the CNT/S cathode into the electrolyte easily, resulting in severe shuttle reactions. However, the shuttle effect appears to be alleviated in the BMC-based cathodes, which can be attributed to the physical confinement and chemical binding of polysulfides at the cathodes.

The rate performance of the BMC/LS and BMC/HS cathodes is presented in Fig. 4(d). Unsurprisingly, the BMC/LS cathode exhibits relatively higher capacities than BMC/HS cathode at each rate due to the lower sulfur loading. The initial discharge capacities of the BMC/LS cathode at 0.16, 0.32, 0.8, 1.6, 3.2, and 8 A/g are 1,255.6, 943.3, 777.6, 650.9, 595.7, and 477.4 mAh/g, and the capacity can be recovered to 820.4 mAh/g when the current rate is back to 0.32 A/g. These results demonstrate that rapid electronic/ionic transport can be achieved in these cathodes. Figure 4(e) shows the cycle performance of the BMC/LS cathode at 3.2 A/g. At the beginning of its cycle, the cell undergoes a reactivation process and the discharge capacity in the first 54 cycles increases. We assume that this increase results from the inability of the sulfur to solve into the electrolyte fast enough [32]. The highest discharge capacity (749.5 mAh/g) was obtained at the 54^{th} cycle. After 500 cycles, the discharge capacity is 561.8 mAh/g, corresponding to a capacity retention of 74.96%. With a very small average capacity decay of 0.056% per cycle during cycling, the Coulombic efficiency remains above 97%. Indeed, it is evident that excellent electrochemical performance can be obtained using the boron-doped carbon host.

In order to elucidate the role of the boron-doped structure in improving the performance of the cells, we performed DFT calculations to study the interaction between the carbon surface and lithium polysulfide species. For simplicity, we used a carbon layer (containing 54 carbon atoms, with hydrogen atoms added to the edges to maintain electrical neutrality) and Li_2S_3 as the models. Detailed descriptions of our computational methods are provided in the Experimental section. While this simulation might not give us an absolute quantification of the binding strength, it will provide a qualitative understanding of the influence of chemical bonding (based on boron) on the cycle performance of the sulfur cathode. Figure 5(a) shows the optimized geometries of the boron-doped and undoped carbon layers and the Li_2S_3 molecule. The corresponding isosurfaces of the cross-sectional density difference and the optimized atomic charges of specific atoms reveal that the electron density is shifted toward the carbon around the boron atoms. This shift can be attributed to the lower electronegativity of boron compared to carbon, a difference that causes the boron atoms to be positively polarized. Besides, the oxygen atoms introduced by boron-doping are likely to further intensify the migration of the electron density away from the boron atoms. Consequently, these positively polarized atoms can attract the negatively charged polysulfides.

In order to confirm the effect of boron-doping on the cell performance, the interactions between raw or boron-doped carbon layers and the polysulfides were studied. Figure 5(b) shows the optimized geometries of a single Li_2S_3 molecule adsorbed on the boron-doped (or undoped) carbon surface, with the corresponding binding energy values listed under the models. Note that boron-doped species are well-known to possess higher binding energies (0.0796, 0.0801, and 0.0803 Ha) than the pristine species (0.0577 Ha), indicating that the boron-doped carbon material exhibits much stronger interactions with the polysulfides species. We also believe that the interaction between polysulfides and the boron-doped carbon is effective only if the size of Li_2S_3 is very small. In our case, the pore structure of BMC is around 0.34 nm (Fig. 1(f)), which confines the growth of polysulfides. Without this unique micropore structure, we doubt there would be any improvement in the electrochemical cycle performance. Besides, the amount of transferred charge on the sulfur atoms adsorbed on the boron-doped carbon surfaces is higher than that on the raw carbon surface. This result further demonstrates that the interaction between polysulfides and the boron-doped carbon is much stronger [33] than the interaction

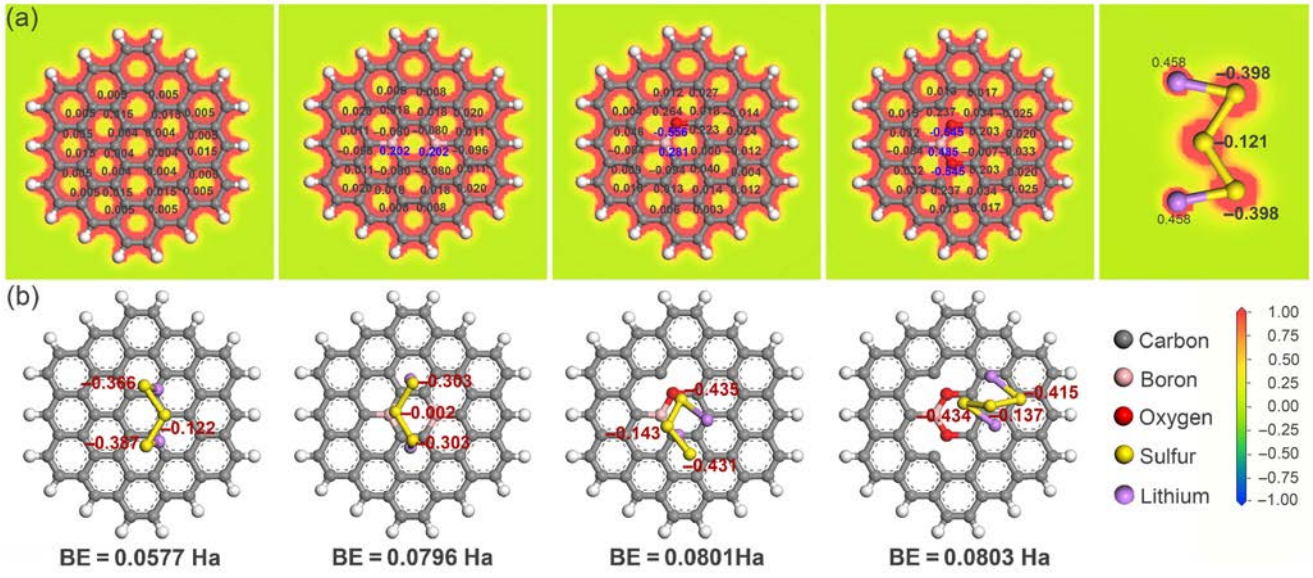

Figure 5 (a) Optimized geometries of the boron-doped and undoped carbon layers and Li_2S_3 molecule and the isosurfaces of the cross-sectional density difference. (b) Top views of Li_2S_3 molecule adsorbed on the boron-doped and boron-undoped carbon surface, and the corresponding binding energy values. The optimized atomic charges of specific atoms are also provided here, and the charge distribution on each atom is evaluated using the Mulliken population analysis.

with undoped carbon. Overall, the boron-doped carbon can adsorb polysulfides more efficiently, thus preventing them from dissolving into the electrolyte, and resulting in an improved cycling performance.

4 Conclusions

In summary, we have successfully developed a boron-doped carbon-based sulfur cathode for high-performance Li-S batteries. The cathode was shown to exhibit an ultra-high cycling stability and rate capability. A maximum discharge capacity of 749.5 mAh/g was obtained at 3.2 A/g (54^{th} cycle), with 561.8 mAh/g remaining after 500 cycles. This decrease corresponds to a very small capacity decay of 0.056% per cycle, with a coulombic efficiency remaining above 97%. The excellent reversibility and stability of BMC-based cathode is attributed to (i) the microporous matrix, which can physically confine polysulfides, (ii) the B-doped polar host, which has a high affinity for polysulfides, and can thus chemically bind these species within the carbon matrix. In good agreement with the experimental observations, the first-principles calculations revealed that boron-doping results in the polarization of the carbon surface and an increase in the binding energy. These results demonstrate that the interaction between the B-doped carbon and polysulfides is stronger than the corresponding interaction with undoped carbon. We believe that the described strategy presents a new material platform that can be applied to other energy storage technologies, such as metal-air batteries and efficient metal-free oxygen reduction reaction (ORR) electrocatalysts for fuel cells.

Acknowledgements

F. W. and J. Q. This work was supported by the National Key Research and Development Program "New Energy Project for Electric Vehicle" (No. 2016YFB0100204), the National Natural Science Foundation of China (No. 21373028), Major achievements Transformation Project for Central University in Beijing, Beijing Science and Technology Project (No. D151100003015001) and the Ford University Research Program (URP) project. W. P. W. acknowledges support from George Daniels Educational Trust.

Electronic Supplementary Material: Supplementary material (further material characterization and detailed

electrochemical analysis) is available in the online version of this article at http://dx.doi.org/10.1007/s12274-016-1303-7.

References

[1] Armand, M.; Tarascon, J. M. Building better batteries. *Nature* **2008**, *451*, 652–657.

[2] Bruce, P. G.; Freunberger, S. A.; Hardwick, L. J.; Tarascon, J. M. Li-O_2 and Li-S batteries with high energy storage. *Nat. Mater.* **2012**, *11*, 19–29.

[3] Manthiram, A.; Fu, Y. Z.; Su, Y. S. Challenges and prospects of lithium–sulfur batteries. *Acc. Chem. Res.* **2013**, *46*, 1125–1134.

[4] Yin, Y. X.; Xin, S.; Guo, Y. G.; Wan, L. J. Lithium-sulfur batteries: Electrochemistry, materials, and prospects. *Angew. Chem., Int. Ed.* **2013**, *52*, 13186–13200.

[5] Yang, Y.; Zheng, G. Y.; Cui, Y. Nanostructured sulfur cathodes. *Chem. Soc. Rev.* **2013**, *42*, 3018–3032.

[6] Liu, M. N.; Ye, F. M.; Li, W. F.; Li, H. F.; Zhang, Y. G. Chemical routes toward long-lasting lithium/sulfur cells. *Nano Res.* **2016**, *9*, 94–116.

[7] Zhou, G. M.; Wang, D.-W.; Li, F.; Hou, P.-X.; Yin, L. C.; Liu, C.; Lu, G. Q.; Gentle, I. R.; Cheng, H.-M. A flexible nanostructured sulphur–carbon nanotube cathode with high rate performance for Li-S batteries. *Energy Environ. Sci.* **2012**, *5*, 8901–8906.

[8] Sun, L.; Li, M. Y.; Jiang, Y.; Kong, W. B.; Jiang, K. L.; Wang, J. P.; Fan, S. S. Sulfur nanocrystals confined in carbon nanotube network as a binder-free electrode for high-performance lithium sulfur batteries. *Nano Lett.* **2014**, *14*, 4044–4049.

[9] Xu, G. Y.; Yuan, J. R.; Tao, X. Y.; Ding, B.; Dou, H.; Yan, X. H.; Xiao, Y.; Zhang, X. G. Absorption mechanism of carbon-nanotube paper-titanium dioxide as a multifunctional barrier material for lithium-sulfur batteries. *Nano Res.* **2015**, *8*, 3066–3074.

[10] Wu, F.; Qian, J.; Chen, R. J.; Zhao, T.; Xu, R.; Ye, Y. S.; Li, W. H.; Li, L.; Lu, J.; Amine, K. Sulfur cathode based on layered carbon matrix for high-performance Li–S batteries. *Nano Energy* **2015**, *12*, 742–749.

[11] Wang, Z. Y.; Dong, Y. F.; Li, H. J.; Zhao, Z. B.; Wu, H. B.; Hao, C.; Liu, S. H.; Qiu, J. S.; Lou, X. W. Enhancing lithium-sulphur battery performance by strongly binding the discharge products on amino-functionalized reduced graphene oxide. *Nat. Commun.* **2014**, *5*, 5002.

[12] Qiu, Y. C.; Li, W. F.; Li, G. Z.; Hou, Y.; Zhou, L. S.; Li, H. F.; Liu, M. N.; Ye, F. M.; Yang, X. W.; Zhang, Y. G. Polyaniline-modified cetyltrimethylammonium bromide-graphene oxide-sulfur nanocomposites with enhanced performance for lithium-sulfur batteries. *Nano Res.* **2014**, *7*, 1355–1363.

[13] Sun, H.; Xu, G. L.; Xu, Y. F.; Sun, S. G.; Zhang, X. F.; Qiu, Y. C.; Yang, S. H. A composite material of uniformly dispersed sulfur on reduced graphene oxide: Aqueous one-pot synthesis, characterization and excellent performance as the cathode in rechargeable lithium-sulfur batteries. *Nano Res.* **2012**, *5*, 726–738.

[14] Zhang, B.; Qin, X.; Li, G. R.; Gao, X. P. Enhancement of long stability of sulfur cathode by encapsulating sulfur into micropores of carbon spheres. *Energy Environ. Sci.* **2010**, *3*, 1531–1537.

[15] Ding, B.; Yuan, C. Z.; Shen, L. F.; Xu, G. Y.; Nie, P.; Zhang, X. G. Encapsulating sulfur into hierarchically ordered porous carbon as a high-performance cathode for lithium-sulfur batteries. *Chem.—Eur. J.* **2013**, *19*, 1013–1019.

[16] Zhang, K.; Zhao, Q.; Tao, Z. L.; Chen, J. Composite of sulfur impregnated in porous hollow carbon spheres as the cathode of Li-S batteries with high performance. *Nano Res.* **2013**, *6*, 38–46.

[17] Ahn, W.; Kim, K.-B.; Jung, K.-N.; Shin, K.-H.; Jin, C.-S. Synthesis and electrochemical properties of a sulfur-multi walled carbon nanotubes composite as a cathode material for lithium sulfur batteries. *J. Power Sources* **2012**, *202*, 394–399.

[18] Chen, J. J.; Zhang, Q.; Shi, Y. N.; Qin, L. L.; Cao, Y.; Zheng, M. S.; Dong, Q. F. A hierarchical architecture S/MWCNT nanomicrosphere with large pores for lithium sulfur batteries. *Phys. Chem. Chem. Phys.* **2012**, *14*, 5376–5382.

[19] Zhao, Y.; Yang, L. J.; Chen, S.; Wang, X. Z.; Ma, Y. W.; Wu, Q.; Jiang, Y. F.; Qian, W. J.; Hu, Z. Can boron and nitrogen co-doping improve oxygen reduction reaction activity of carbon nanotubes? *J. Am. Chem. Soc.* **2013**, *135*, 1201–1204.

[20] Wang, S. Y.; Zhang, L. P.; Xia, Z. H.; Roy, A.; Chang, D. W.; Baek, J. B.; Dai, L. M. BCN graphene as efficient metal-free electrocatalyst for the oxygen reduction reaction. *Angew. Chem., Int. Ed.* **2012**, *51*, 4209–4212.

[21] Kruk, M.; Jaroniec, M. Gas adsorption characterization of ordered organic-inorganic nanocomposite materials. *Chem. Mater.* **2001**, *13*, 3169–3183.

[22] Wu, F.; Qian, J.; Chen, R.; Lu, J.; Li, L.; Wu, H.; Chen, J.; Zhao, T.; Ye, Y.; Amine, K. An effective approach to protect lithium anode and improve cycle performance for Li-S batteries. *ACS Appl. Mater. Interfaces* **2014**, *6*, 15542–15549.

[23] Chen, R. J.; Zhao, T.; Lu, J.; Wu, F.; Li, L.; Chen, J. Z.; Tan, G. Q.; Ye, Y. S.; Amine, K. Graphene-based three-dimensional hierarchical sandwich-type architecture for high-performance Li/S batteries. *Nano Lett.* **2013**, *13*, 4642–4649.

[24] Ferrari, A. C.; Robertson, J. Interpretation of Raman spectra of disordered and amorphous carbon. *Phys. Rev. B* **2000**, *61*, 14095–14107.

[25] Katagiri, G.; Ishida, H.; Ishitani, A. Raman spectra of graphite edge planes. *Carbon* **1988**, *26*, 565–571.

[26] Ward, A. T. Raman spectroscopy of sulfur, sulfur-selenium, and sulfur-arsenic mixtures. *J. Phys. Chem.* **1968**, *72*, 4133–4139.

[27] Moulder, J. F.; Chastain, J.; King, R. C. *Handbook of X-ray Photoelectron Spectroscopy*; Perkin-Elmer Corporation: Eden Prairie, MN, USA, 1992.

[28] Panchakarla, L. S.; Subrahmanyam, K. S.; Saha, S. K.; Govindaraj, A.; Krishnamurthy, H. R.; Waghmare, U. V.; Rao, C. N. R. Synthesis, structure, and properties of boron- and nitrogen-doped graphene. *Adv. Mater.* **2009**, *21*, 4726–4730.

[29] Ennaceur, M. M.; Terreault, B. XPS study of the process of oxygen gettering by thin films of PACVD boron. *J. Nucl. Mater.* **2000**, *280*, 33–38.

[30] Akridge, J. R.; Mikhaylik, Y. V.; White, N. Li/S fundamental chemistry and application to high-performance rechargeable batteries. *Solid State Ionics* **2004**, *175*, 243–245.

[31] Zhang, S. S. Role of $LiNO_3$ in rechargeable lithium/sulfur battery. *Electrochim. Acta* **2012**, *70*, 344–348.

[32] Koh, J. Y.; Park, M. S.; Kim, E. H.; Kim, T. J.; Kim, S.; Kim, K. J.; Kim, Y. J.; Jung, Y. Electrochemical reduction mechanism of sulfur particles electrically isolated from carbon cathodes of lithium-sulfur cells. *J. Electrochem. Soc.* **2014**, *161*, A2117–A2120.

[33] Zhou, G. M.; Yin, L. C.; Wang, D. W.; Li, L.; Pei, S. F.; Gentle, I. R.; Li, F.; Cheng, H. M. Fibrous hybrid of graphene and sulfur nanocrystals for high-performance lithium-sulfur batteries. *ACS Nano* **2013**, *7*, 5367–5375.

Table of contents

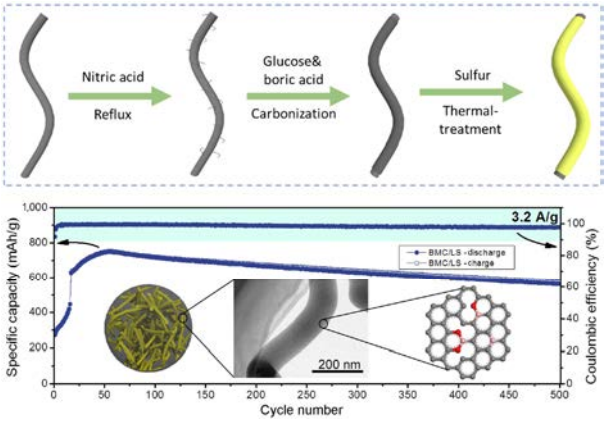

A boron-doped microporous carbon (BMC)/sulfur composite is synthesized and applied successfully as a novel cathode material for advanced Li-S batteries.

Electronic Supplementary Material

Boron-doped microporous nano carbon as cathode material for high-performance Li-S batteries

Feng Wu[1,2,§], Ji Qian[1,§], Weiping Wu[3], Yusheng Ye[1], Zhiguo Sun[1], Bin Xu[4], Xiaoguang Yang[5], Yuhong Xu[6], Jiatao Zhang[7], and Renjie Chen[1,2] (✉)

[1] *Beijing Key Laboratory of Environmental Science and Engineering, School of Material Science and Engineering, Beijing Institute of Technology, Beijing 100081, China*

[2] *Collaborative Innovation Center of Electric Vehicles in Beijing, Beijing 100081, China*

[3] *School of Computer Science, Mathematics and Engineering, City, University of London, Northampton Square, London, EC1V 0HB, UK*

[4] *State Key Laboratory of Chemical Resource Engineering, Beijing Key Laboratory of Electrochemical Process and Technology for Materials, Beijing University of Chemical Technology, Beijing 100029, China*

[5] *Research and Advanced Engineering, Ford Motor Company, MI 48121, USA*

[6] *Electrified Powertrain Engineering, Ford Motor Research and Engineering (Nanjing) Co. Ltd., Nanjing 211100, China*

[7] *Beijing Key Laboratory of Construction-Tailorable Advanced Functional Materials and Green Applications, School of Material Science and Engineering, Beijing Institute of Technology, Beijing 100081, China*

[§] *These authors contributed equally to this work.*

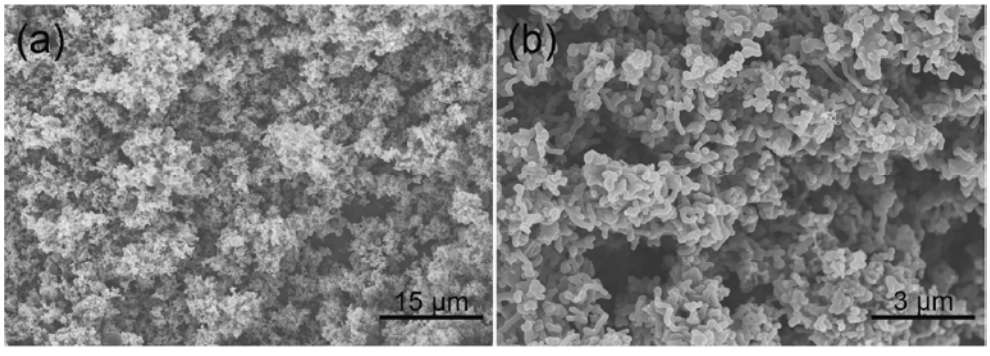

Figure S1 Low magnification SEM images of BMC.

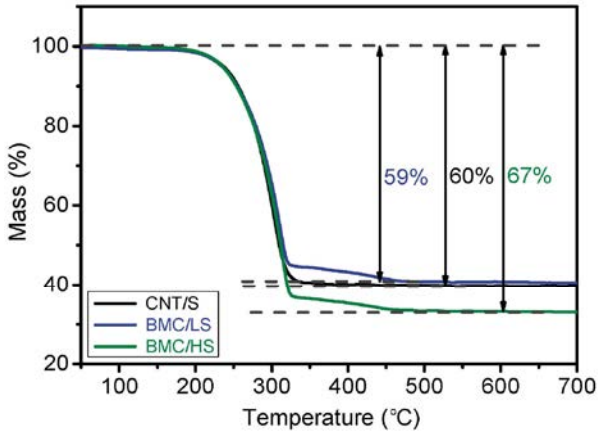

Figure S2 TGA curves of the CNT/S, BMC/LS and BMC/HS composites recorded in Ar at a heating rate of 10 ˚C/min.

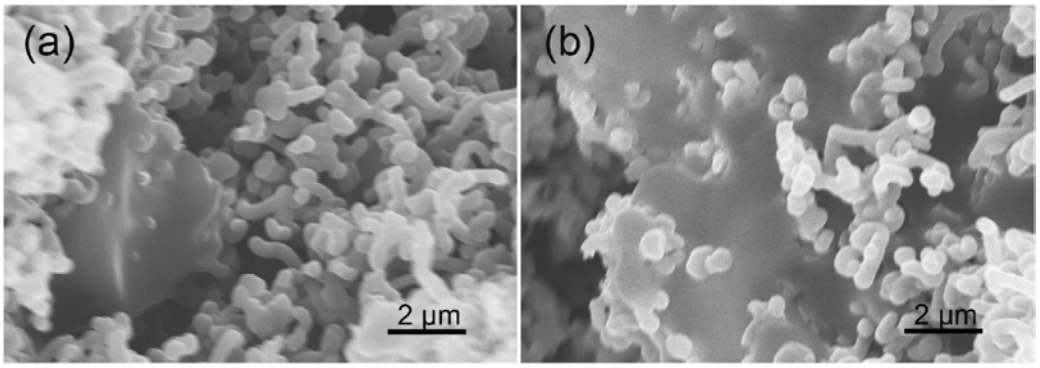

Figure S3 SEM image of the sulfur-BMC composite obtained with only 8 h thermal treatment.

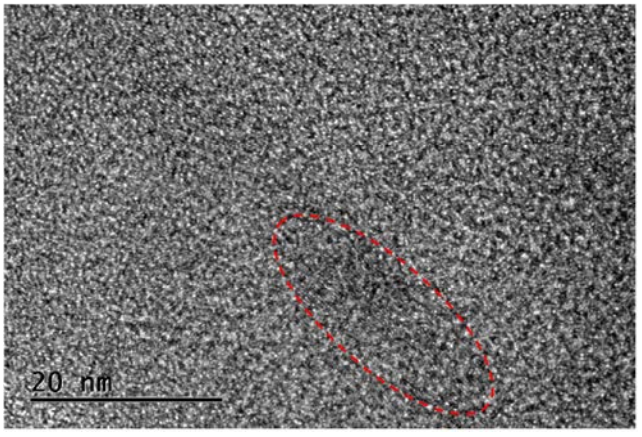

Figure S4 HRTEM image of the BMC/LS composite. The lattice strings of CNTs are marked by the dotted ellipse.

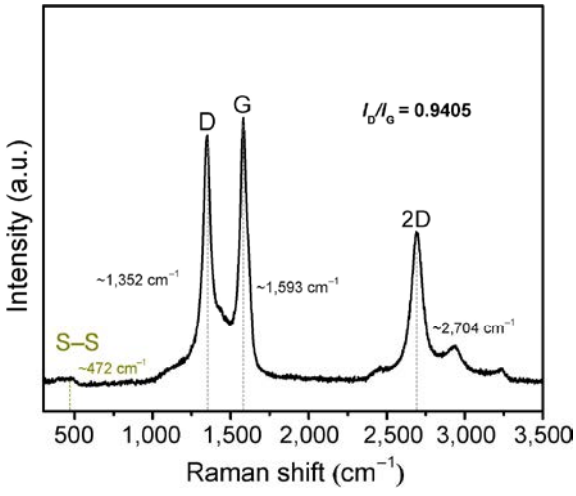

Figure S5 Raman spectrum of the CNT/S composite.